Supplementary Materials for

Electrical Tissue Adhesive for Strain-insensitive In-situ Biosensing

This PDF file includes:

Supplementary notes

Figure S1 to S21

Table S1

Notes for movies

Other Supplementary Material for this manuscript includes the following:

Movie S1

Movie S2

Supplementary Notes

Materials

All chemicals were obtained from Sigma-Aldrich unless otherwise mentioned and used without further purification. To prepare the electrical tissue adhesive, gelatin methacrylate (gelMA; type A, bloom 90-100 from porcine skin with 60% substitution), acrylic acid N-hydroxysuccinimide ester (AAc-NHS ester), gelatin (type A, bloom 300 from porcine skin), α-ketoglutaric acid, and acrylic acid were used. The following materials were used to fabricate the glucose sensor: polyimide (PI) film (5 mil thickness, Kapton), poly(pyromellitic dianhydride-co-4,4'-oxydianiline), amic acid solution, chloroplatinic acid, lead acetate, glutaraldehyde (GA), glucose oxidase (GOx), chitosan, silver/silver chloride (Ag/AgCl paste, purchased from Shanghai Julong Electronic Technology Co., Ltd.), and hexamethyldiamine (HMDA). Porcine tissues were purchased from a research level biological tissue vendor (Sierra For Medical Science).

Synthesis

To synthesize the electrical tissue adhesive, 10% (w/w) gelatin, 30% (w/w) acrylic acid, and 0.1% (w/w) GelMA were dissolved in deionized water (DI water) using magnetic stirring at 80°C for 4 hours until fully dissolved. Subsequently, 0.2% (w/w) α-ketoglutaric acid and 1% (w/w) AAc-NHS ester were added to the mixture. This hydrogel precursor was then sandwiched between two quartz glasses pre-treated with a water repellent, using two layers of parafilm (approximately 250 μm thick) as spacers. The hydrogel precursor was then exposed to UV light (365 nm) in an incubator (UVP CL-1000) for 30 minutes. The thickness of the cured hydrogel was controlled by varying the number of parafilm layers. Afterwards, the hydrogel was left to air-dry for 12 hours, then sealed with desiccant and stored in a -25°C refrigerator for preservation.

Fabrications

Fabrication of the polyimide-gold electrodes. To fabricate the polyimide-gold electrodes for the glucose sensors, PI films were initially cut into dimensions of 5 cm × 7.5 cm, and cleaned sequentially with ethanol and DI water. After drying with a nitrogen flow, the films were affixed to quartz glasses using double-sided tape. To improve the interaction between the PI film and gold, poly(pyromellitic dianhydride-co-4,4'-oxydianiline), amic acid solution was spin-coated onto the films at 3000 rpm for 30 seconds, followed by incubation at 250 °C for 30 minutes [1]. Subsequently, a 100 nm layer of gold was sputtered onto the coated PI film. The PI-gold film was then cut into the designed configuration using either a laser cutter (Epilog) or a cutting machine (Brother ScanNCut CM350).

Amine functionalization of polyimide film. To functionalize the PI films with amine groups, the electrodes were first cleaned with ethanol and DI water, dried with a nitrogen flow, and then immersed in HMDA solution (10% w/w in DI water) for 24 hours at room temperature [2]. The

electrodes were then rinsed with DI water and dried with a nitrogen flow for preservation (Figure S1).

Surface functionalization of gold electrodes. To fabricate the electrochemical glucose biosensor, the gold surface of a polyimide-gold electrode, serving as the working electrode, was initially electrodeposited with platinum black at a constant voltage of -0.8 V for 3 minutes using an electrolyte containing 24×10^{-3} mol/L chloroplatinic acid and 2.1×10^{-3} mol/L lead acetate, controlled by the electrochemical workstation (Biologic SP-150e). Subsequently, it was gently cleaned with DI water by pipette. Following this, a 10 μL mixture of glucose oxidase (Gox, 2.5 U/μL), chitosan (1% w/w), and glutaraldehyde (GA, 1% w/w) in a 1:1:1 ratio was drop-cast onto the platinum black surface and left overnight at 4°C, covered with aluminum foil [3]. For the reference electrode, a thin layer of Ag/AgCl paste was screen-printed onto the gold surface and dried at 80°C for 30 minutes (Figure S2) (For the lactate sensor, glucose oxidase is replaced by lactate oxidase).

Assembly of the glucose biosensor and the electrical tissue adhesive. To assemble the glucose biosensor (1 cm × 2 cm) with the electrical tissue adhesive (7.5 cm × 5 cm), the biosensor was initially cleaned with DI water and then affixed onto the electrical tissue adhesive by a gentle compressive force for approximately five seconds. Any remaining water molecules on the PI film surface were absorbed by the dry electrical tissue adhesive, facilitating adhesion through covalent crosslinks between the amine groups grafted on the PI and the PAAc-NHS ester in the electrical tissue adhesive.

Mechanical characterizations of electrical tissue adhesives

Adhesion characterization of the porcine skin and the PI film adhered by the electrical tissue adhesive. For the adhesion tests, both the porcine skin and the amine-functionlized PI film were cut into 2 cm × 4 cm pieces and cleaned with ethanol and DI water. A 1 cm × 4 cm layer of tissue adhesive hydrogel was then placed between the porcine skin and the PI film, followed by a gentle compressive force for approximately five seconds to ensure conformal contact among the three layers (Figure S6). The resulting sandwitch structure (i.e., porcine skin, tissue-adhesive hydrogel, and PI film) was left in an ambient environment for a controlled adhesion time t_a before characterization. To measure the interfacial toughness between the porcine skin and the PI film adhered by the tissue adhesive hydrogel, we adopted a T-peel test following the ASTM D1876. Specifically, a 2 cm × 5 cm PI film was attached to the back of the procine skin as a stiff backing layer. Additionaly, two 1 cm × 0.5 cm acrylic pieces were attached on both PI films to serve as holders for the U-Stretch testing device clips. One end of the T-peel specimen was fixed, while the other end was stretched vetically at a speed of 1 mm/s. The same procedure was followed for the samples exposed to ambient air for 24 hours and those immersed in a water bath for 15 minutes.

Bulk characterization of the electrical tissue adhesive. All mechanical tests were conducted using a U-Stretch testing device (CellScale). For the uniaxial stretching test, a 3 cm × 2 cm electrical tissue adhesive in its dry state was glued between two 3 cm × 2 cm acrylic pieces, with 1 cm × 0.5 cm acrylic pieces attached at the ends as holders, leaving a height of 1 cm of the electrical tissue adhesive for stretching. The assembly was immersed in DI water for rehydration for a controlled hydration time (t_h), then clipped onto the UStretch testing machine and stretched vertically at a rate of 1 mm/s until it broke. The same procedure was applied to the notched hydrogel sample, which contains a 1 cm notch introduced in the middle of the hydrogel film. For the measurement of mechancial hysteresis, the electrical tissue adhesive was retracted after being stretched to a controlled stretch (λ) at the same rate. To calculate fracture toughness and Young's modulus of the electrical tissue adhesive, the fracture toughness was determined from the experimental results of the unnotched and notched hydrogel, with details shown in Figure S8. The Young's modulus was calculated from the initial slope of the stress-stretch curve of the unnotched hydrogel.

Strain sensitivity characterization of the electrical tissue adhesive. To characterize the strain sensitivity of the electrical tissue adhesive adhered with electrodes, a 3 cm × 1 cm electrode and a 7.5 cm × 5 cm electrical tissue adhesive were assembled following the steps outlined in "*Assembly of the glucose sensor and the electrical tissue adhesive*". The electrical tissue adhesive was then glued between two 3 cm × 2 cm acrylic pieces, with 1 cm × 0.5 cm acrylic pieces attached at the ends as holders. Two conductive wires were soldered to the electrode and connected to a multimeter (DAQ970A). Various deformations (i.e., stretching, twisting, and bending) were applied onto the electrical tissue adhesive. For stretching, the steps outlined in "*Bulk characterization of the electrical tissue adhesive*" were followed. The electrical hysteresis was measured by simultaneously recording the changes in electrical conductivity and the stretching of the electrical tissue adhesive. Additionally, the samples were stretched at different frequencies to determine the relationship between stretching frequency and electrical conductivity.For twisting, it was achieved rotating one of the clips on the U-Stretch testing device. For bending, the electrical tissue adhesive was placed on a thin glass rod and bent along the rod to different angles. The resistance of the electrode was measured as the electrical tissue adhesive was deformed to different extents. The change in electrical conductivity of the electrode was calculated using the formula $(R_1 - R_0) / R_0$, where R_0 was the resistance in its undeformed state and R_1 was the resistance in its deformed state.

Finate element simulation of electrical tissue adhesives

Simulation of crack propagation in an electrical tissue adhesive. The finite element simulation for simulating crack propagation in an electrical tissue adhesive was conducted using ABAQUS/Explicit (Figure S12). Initially, the material's nonlinear large deformation was characterized using the second-order Ogden model with its strain energy density reading as

$$W = \sum_{i=1}^{2} 2\mu_i/\alpha_i^2(\lambda_1^{\alpha_i} + \lambda_2^{\alpha_i} + \lambda_3^{\alpha_i} - 3)$$

where W represents the strain energy density, λ_1, λ_2, λ_3 were the three principal stretch ratios, μ_1 and μ_2 denoted shear moduli, and α_1 and α_2 were material constants. Secondly, to capture the dissipation effects in the process zone, Mullins-effect models were incorporated into the material, resulting in hysteresis loops in the stress-stretch curves during loading-unloading cycles. To extract the material constants associated with the Ogden model and the Mullins-effect model, we implemented these two models into a two-dimensional specimen in Abaqus to simulate the loading-unloading stress-stretch curves under different stretch ratios (Figure S9) [3]. The geometry of the specimen was set as 30 mm in width and 10 mm in length. Finally, a coupled Ogden model, Mullins-effect model, and cohesive-zone model were implemented to simulate the crack propagation of the material under pure shear tensile loading (Figure S11). The cohesive-zone model was used to define the failure of the material, characterized by the maximum stress S_{max} and the maximum separation δ_{max}. The maximum stress S_{max} was taken as the measured nominal stress at failure of the electrical tissue adhesive under pure shear test, and the maximum separation δ_{max} was identified using $\delta_{max} = 2\Gamma / S_{max}$ with Γ being the fracture toughness of the electrical tissue adhesive after subjected to 1000 cycles of loading (Figure S10). The geometry of the notched specimen was 30 mm × 10 mm × 0.26 mm with a crack length of 10 mm. The electrical tissue adhesive was modeled using plane-stress 4-node linear elements. The material was loaded along vertical direction with a constant velocity 0.1 mm/s.

Simulation of strain-sensitivity of an electrical tissue adhesive adhered with an electrode. The finite element simulation for simulating strain-sensitivity of an electrical tissue adhesive adhered with an electrode was conducted using ABAQUS/Static (Figure S14 and Movie S1). Both the Ogden model and the Mullins-effect model, employing the same parameters as the fracture simulation, were used for the electrical tissue adhesive. A linear elastic model with Young's modulus E = 2.5 GPa was used for the electrode. The two components were adhered at their interfaces. The electrical tissue adhesive was loaded horizontally at a constant velocity of 0.1 mm/s.

Energy Release rate for Adhesion Tension Test

To compare the energy release rate for electrode-skin adhesion and electrode-hydrogel-skin adhesion, we performed finite element simulations using ABAQUS/Static for both scenarios. The electrode dimensions are 10 mm × 10 mm × 0.127 mm, with an elastic modulus of E = 25 GPa. The hydrogel has dimensions of 10 mm × 10 mm × 0.25 mm and follows a nonlinear-elastic model based on the parameters from the fracture test. The skin has dimensions of 20 mm × 20 mm × 2 mm, modeled as an incompressible Ogden hyperelastic solid, with fitting parameters μ=40 kPa and $\alpha = 20$ [4]. To calculate the energy release rate for electrode-skin adhesion, we first perform a tensile test on the skin with the electrode perfectly adhered to its

surface, obtaining the strain energy U. Next, we simulate the release of the adhered interface between the electrode and skin over a small distance ΔL, keeping all other conditions unchanged. To maintain crack symmetry, the release is initiated from each edge of the electrode-skin interface. The strain energy for the released surface is noted as U'. The energy release rate for interfacial crack propagation is then calculated based on the difference between U and U'.

$$G = \frac{U - U'}{\Delta L}$$

To obtain the energy release rate for the electrode-hydrogel-skin adhesion test, we follow a similar procedure. First, we perform a tensile test on the skin where the electrode is adhered to the hydrogel, and the hydrogel is adhered to the skin surface, obtaining the strain energy for the perfectly adhered surface. Next, we release the adhered interface between the electrode and the hydrogel over a small distance and run the simulation with all other conditions unchanged to calculate the energy release rate $G_{electrode}$. Then, we release the adhered surface between the hydrogel and the skin by the same small distance, perform the simulation with all other conditions unchanged, and calculate the energy release rate $G_{hydrogel}$.

In vitro biocompatibility tests

We performed in vitro biocompatibility assays using electric tissue adhesive-conditioned medium. NIH 3T3 cells were cultured in complete medium composed of Dulbecco's Modified Eagle Medium (DMEM, Life Technologies), supplemented with 10% fetal bovine serum (Sigma-Aldrich) and 1% penicillin/streptomycin (Life Technologies). To prepare the conditioned medium, 60 mg of the gelatin-based electric tissue adhesive was incubated in 2 mL of complete medium at 37°C for 24 hours, with pristine complete medium used as the control. NIH 3T3 cells were seeded into 96-well plates (n = 12 for the electric tissue-conditioned medium; n = 12 for the control medium) and incubated at 37°C with 5% CO2 for 48 hours. Cell viability was then evaluated using the LIVE/DEAD viability/cytotoxicity kit (Life Technologies) according to the manufacturer's protocol. This assay employed 4 μM calcein to stain live cells and ethidium homodimer-1 for dead cells. Imaging was conducted using a Leica SP8 confocal microscope, with live cells detected at excitation/emission wavelengths of 495 nm/515 nm, and dead cells at 495 nm/635 nm.

Electrochemical characterization of the glucose biosensor.

Calibration of the glucose biosensor. The glucose biosensor was connected to the electrochemical workstation, with its sensing parts immersed in a 50 ml 1× PBS solution. The solution was stirred by a magnetic stirrer at 20 rpm to maintain a dynamic balance. Each time, 500 μL of a 10 mM glucose solution was added to the PBS solution and allowed to stabilize for 2 minutes. The open circuit voltage was then measured for 30 seconds to obtain the corresponding electrical signals generated by the glucose sensor.

Calibration of sensing specificity of the glucose biosensor. The same procedure was adopted for measuring the K^+ and Na^+ concentrations. The sensor was cleaned with DI water before

changing the solution.

Sensing characteraization of the glucose biosensor under different stretches and cycle numbers. The electrical tissue adhesive adhered with a glucose biosensor was fabricated and affixed to the U-Stretch testing device following the procedure outlined in "*Strain sensitivity characterization of the electrical tissue adhesive*". The sensing parts of the biosensor were placed in a long container with 200 ml of 1× PBS. Then, 2 ml of 10 mM glucose solution was added to the PBS solution and allowed to stabilize for 2 minutes. The electrical signal was measured at controlled stretches and cycle numbers (Figure S14). The stretching of the electrical tissue adhesive was conducted following the procedure outlined in "*Bulk characterization of the electrical tissue adhesive*". During the measurements of electrical signals, the stretch was paused.

Human subject recuritment

Participants, all aged over 18, were recruited from Michigan State University. Prior to participation, each subject provided written informed consent. The majority of participants had a healthy body condition, with a body mass index (BMI) ranging from 18.5 to 24.9, and one participant had a BMI of 27.5. All subjects maintained a regular exercise routine.

Demonstration of long-term monitoring of daily actitivies

A glucose biosensor was cleaned by DI water, and attached onto a electrical tissue adhesive following the steps outlined in "*Assembly of the glucose biosensor and the electrical tissue adhesive.*". To attach the electrical tissue adhesive onto the skin surface, the skin was cleaned with ethanol and DI water. The electrical tissue adhesive was then placed on the wet surface with gentle pressure for approximately five seconds to ensure conformal contact between the tissue adhesive hydrogel and skin. For measuring glucose concentration in sweat, the electrical tissue adhesive was attached to the skin with sweat serving as the interface liquid. The sensor was connected to the workstation using conductive tapes. During exercise and dieting, the sensor-electrical tissue adhesive remained on the skin surface for subsequent measurements. To measure the change in glucose concentration before and after exercise, the glucose sensor was attached to the subjects' arm at the beginning of exercise. All subjects jogged for 30 minutes without water intake. Afterwards, the sensor was connected to the electrochemical workstation to record the glucose concentration in the sweat of each subject. To measure the change in glucose concentration before and after dieting, all subjects were tested in the morning before consuming any water or food. Another test was conducted 30 minutes after their lunch, which included carbohydrates and sugary drinks. Tests on human skin performed at Michigan State University were approved by the Institutional Review Board (IRB), Michigan State University, and informed written consent was obtained (approval number: STUDY00011110).

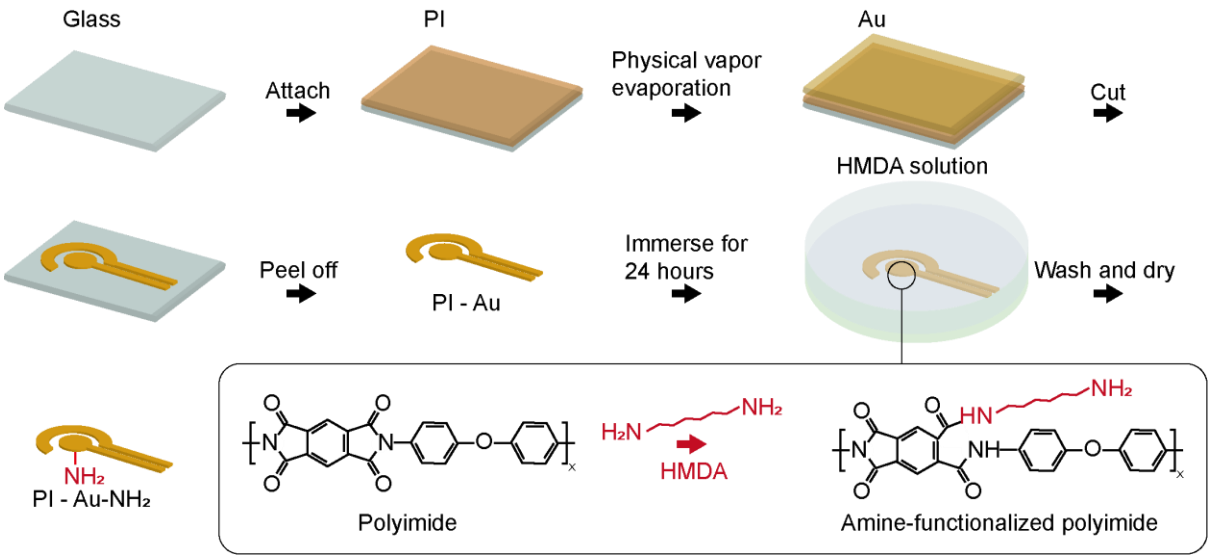


Figure S1. Schematic illustration of the fabrication of the sensing electrode. Schematics of the electrode fabrication process begins with evaporating gold nanoparticles onto a PI film. After cutting the film into the designed shape, the electrode was immersed in an HMDA solution to graft amine groups onto the surface of the PI film.

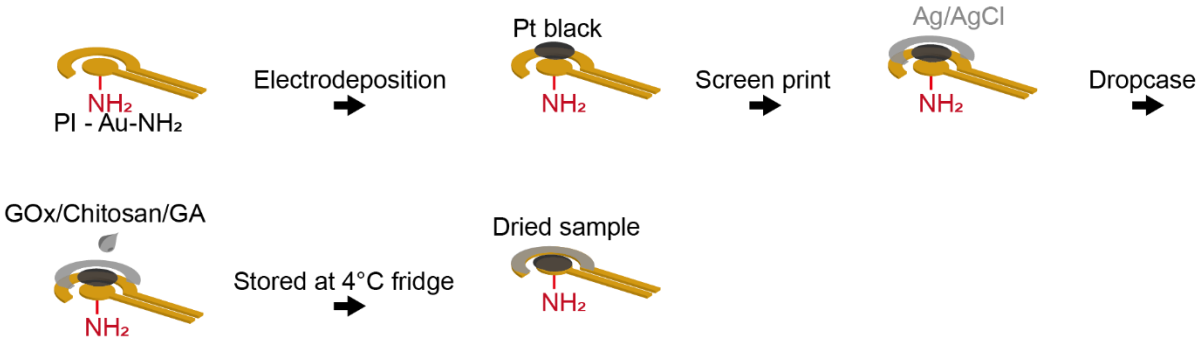


Figure S2. Schematic illustration of the surface functionalization of the electrode. Schematics of the surface functionalization process of the electrode begins with electrodepositing platinum black nanoparticles onto the working electrode and screen-printing silver/silver chloride onto the reference electrode. Next, a mixture of GOx, chitosan, and GA was drop-cast onto the surface of the platinum black and allowed to dry overnight at 4°C fridge.

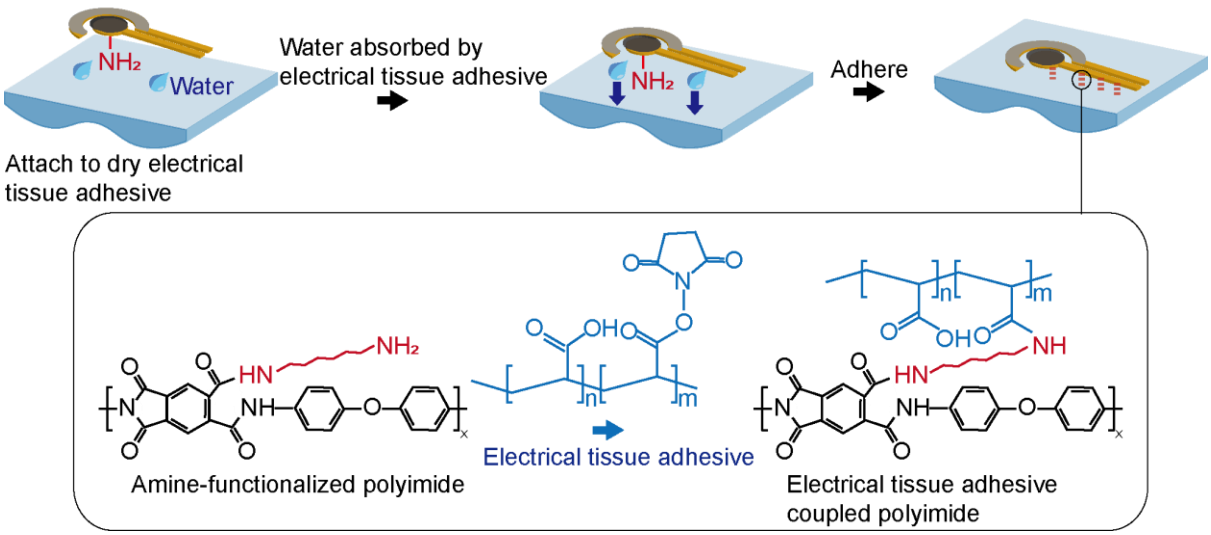


Figure S3. Dry-crosslinking mechanism of the electrical tissue adhesive to biosensor. Schematics of the DI water-cleaned functionalized biosensor being attached to a dry electrical tissue adhesive. As the interfacial water molecules are absorbed, covalent crosslinks are established between the amine-functionalized PI film and the electrical tissue adhesive.

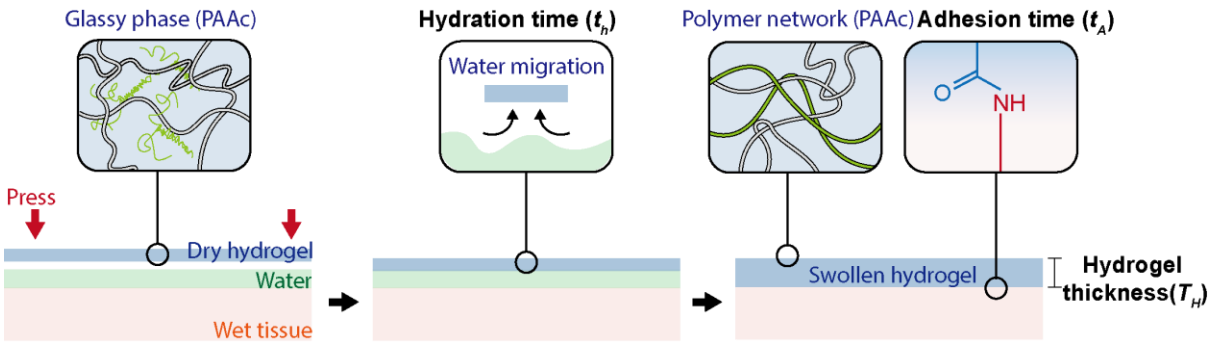


Figure S4. Dry-crosslinking mechanism of the electrical tissue adhesives to wet tissues. The adhesion process starting with a dry electrical tissue adhesive absorbing interfacial water, undergoing phase changes, and establishing covalent crosslinks with tissues. There are three key parameters affecting the adhesion and bulk properties of electrical tissue adhesives: hydration time (t_h), adhesion time (t_a), and hydrogel thickness (T_h).

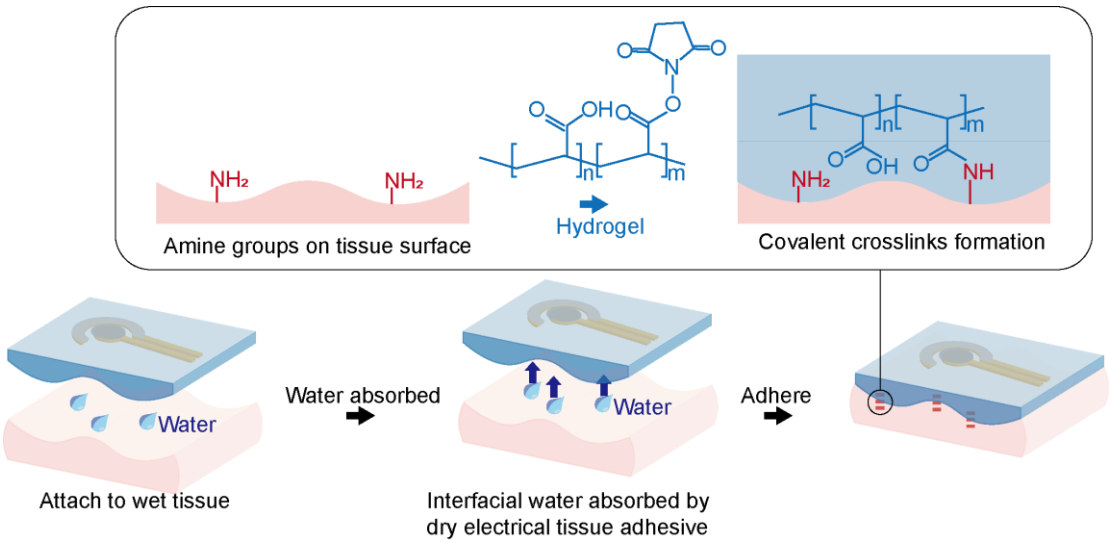


Figure S5. Adhesion procedure of the electrical tissue adhesive onto wet tissues. Schematics of a dry biosensor-electrical tissue adhesive being attached to a wet tissue. As the interfacial water molecules are absorbed, covalent crosslinks are established between the electrical tissue adhesive and the primary amine groups on the tissue.

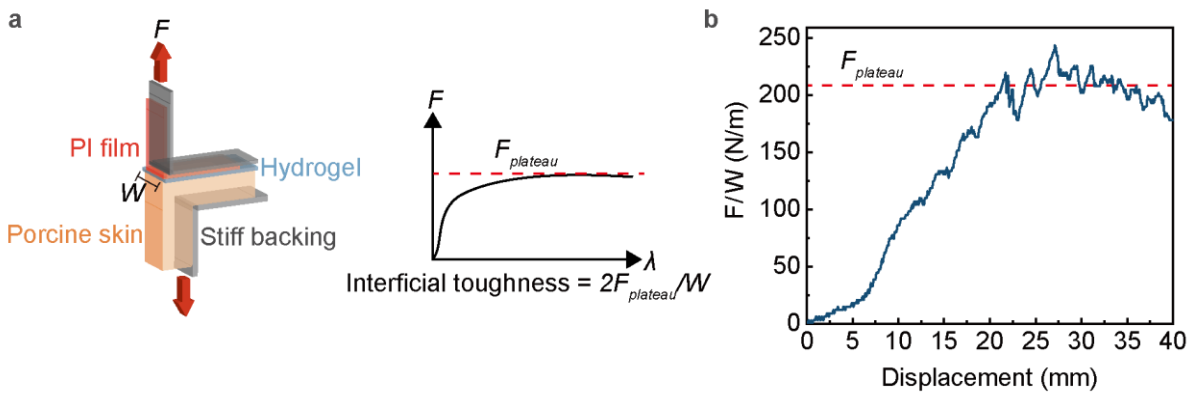


Figure S6. Experimental measurement of the interfacial toughness. a) Schematics of the measurement of interfactil toughness between porcine skin and PI film adhered by the electrical tissue adhesive using a T-peel test. b) A representitive normalized force F/W as a function of peeling displacement, from which $2F_{plateau}/W$ defines the measured interfacuial toughness with $F_{plateau}$ being the steady-state force.

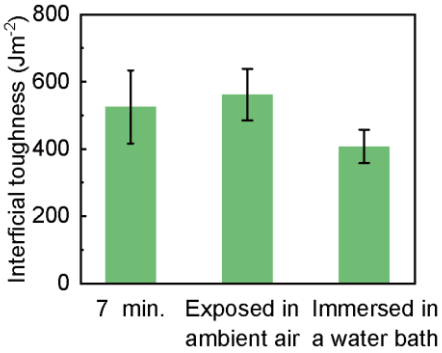


Figure S7. Interfacial toughness between the porcine skin and the PI film adhered by the dry adhesive film with a fixed thickness (T_h = 50 μm), but various conditions including exposed in ambient air for 7 minutes, 24 hours and immersed in a water bath for 15 minutes. Values represent the mean and the standard deviation (n = 3).

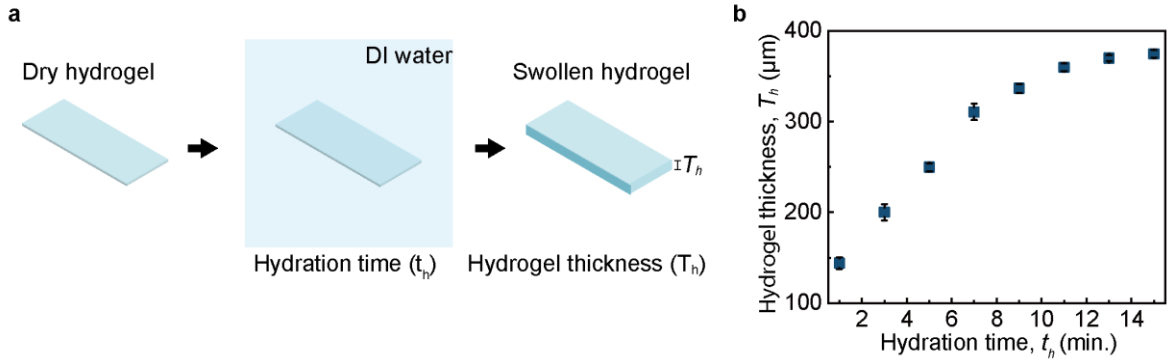


Figure S8. Swelling of the dry electrical tissue adhesive. a) Schematics of the swelling process of the dry electrical tissue adhesive. b) Relationship between hydration time (t_h) and hydrogel thickness (T_h). Values in (b) represent the mean and the standard deviation ($n = 3$).

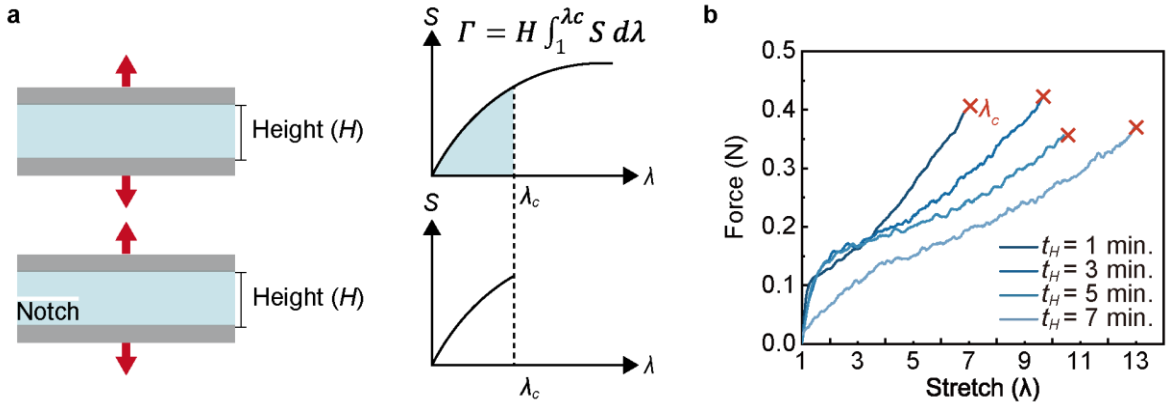


Figure S9. Measurement of the fracture toughness. a) Schematics of pure shear tensile test of an unnotched and a notched specimen to measure the fracture toughness. b) Force-stretch curves of the notched specimens with different hydration time (t_h). The red cross marks the critical point at which the crack in the notched specimen propagates.

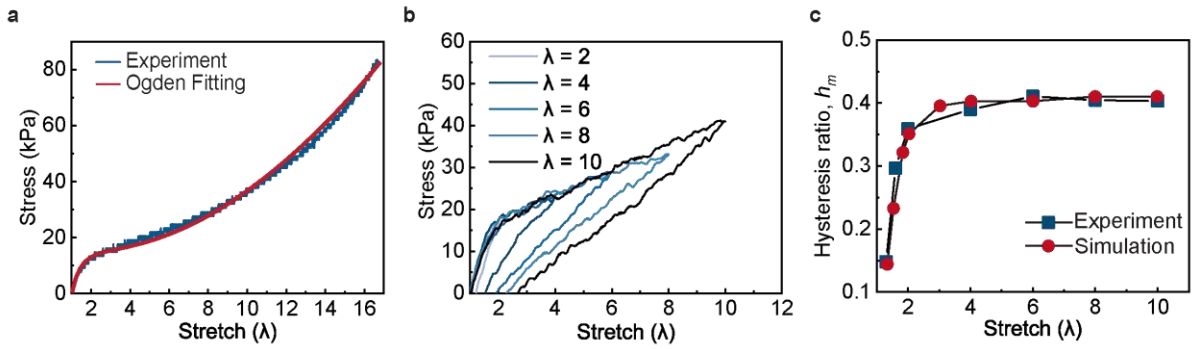


Figure S10. Comparison of experimental and theoretical results of the electrical tissue adhesive under a pure shear test: a) Nominal stress versus stretch curve of an unnotched specimen, showing both experimental result and theoretical calculation (Ogden fitting). b) Nominal stress versus stretch curves of the unnotched specimens under single cycle of loading and unloading during pure shear tensile deformation. c) Comparisons of the hysteresis ratio as a function of stretch between experiment and simulation [5].

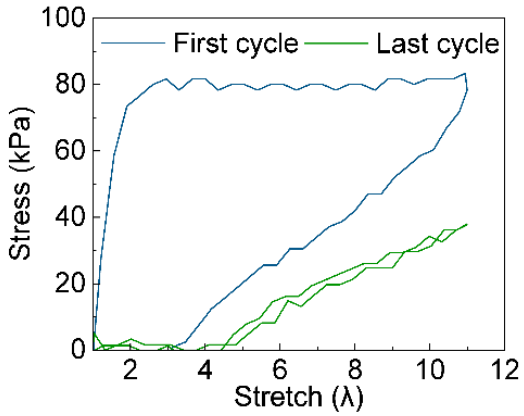


Figure S11. Stress-stretch curve of an electrical tissue adhesive, comparing the first cycle and the last cycle (after 1000 cycles). It demonstrates that in the first cycle, there is a large hysteresis loop, while in the last cycle, the hysteresis loop is negligible.

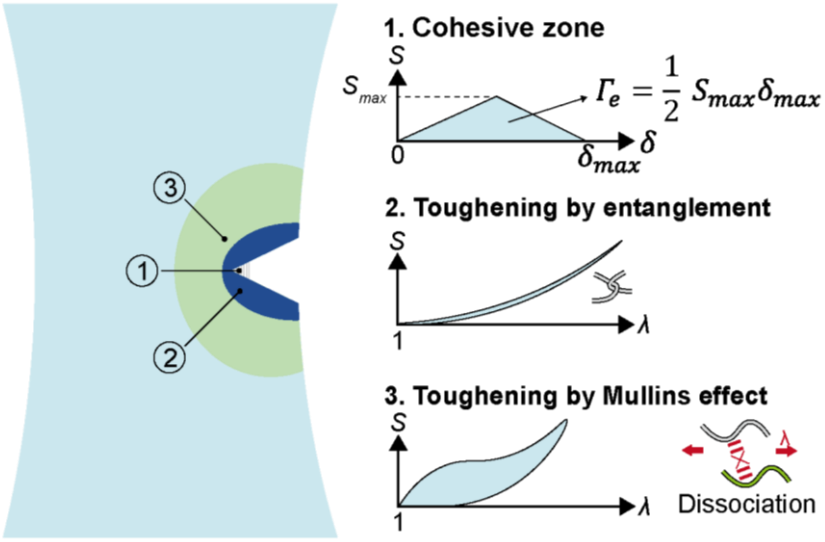


Figure S12. Schematic illustration of the toughening mechanisms of the electrical tissue adhesive. Crack progration in the electrical tissue adhesive is governed by: 1) cohesive zone, 2) low-hysteresis toughening by molecular entanglements, and 3) high-hysetersis toughening by Mullins effect.

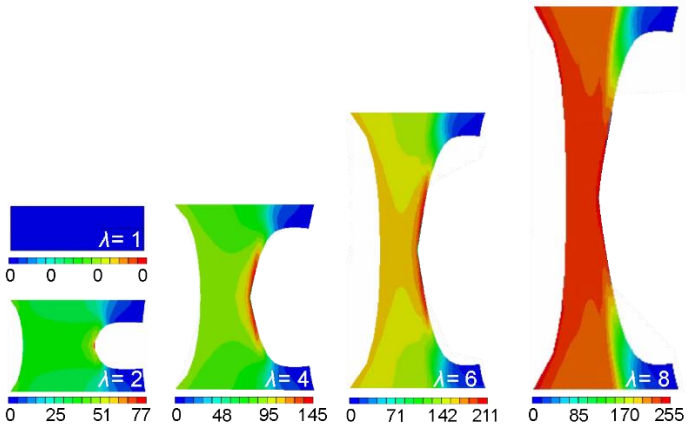


Figure S13. Finite Element Analysis of a notched specimen under pure shear tensile test. Simulation of a crack initiating, blunting, and propagation in a notched specimen.

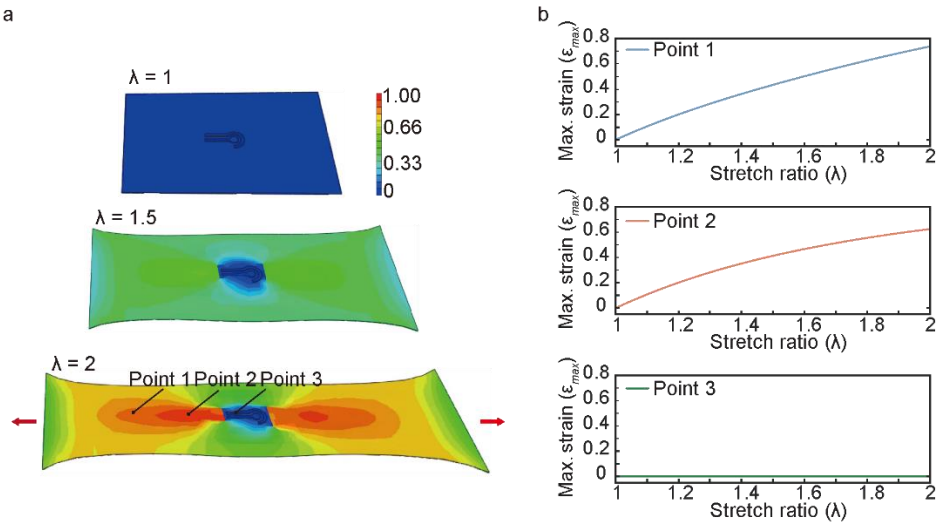


Figure S14. a) Finite Element Analysis of an electrical tissue adhesive adhered with electrode under stretching. The strain in the electrical tissue adhesive varies at different locations (b), whereas the strain in the electode is neglgible.

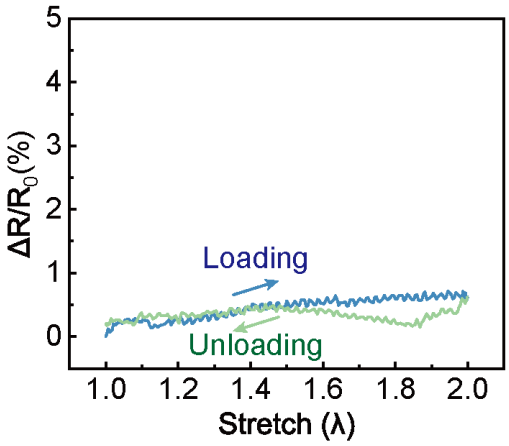


Figure S15. The variation in the gold electrode's electrical conductivity $\Delta R/R_0$ as a function of the applied loading and unloading cycle of the electrical tissue adhesive.

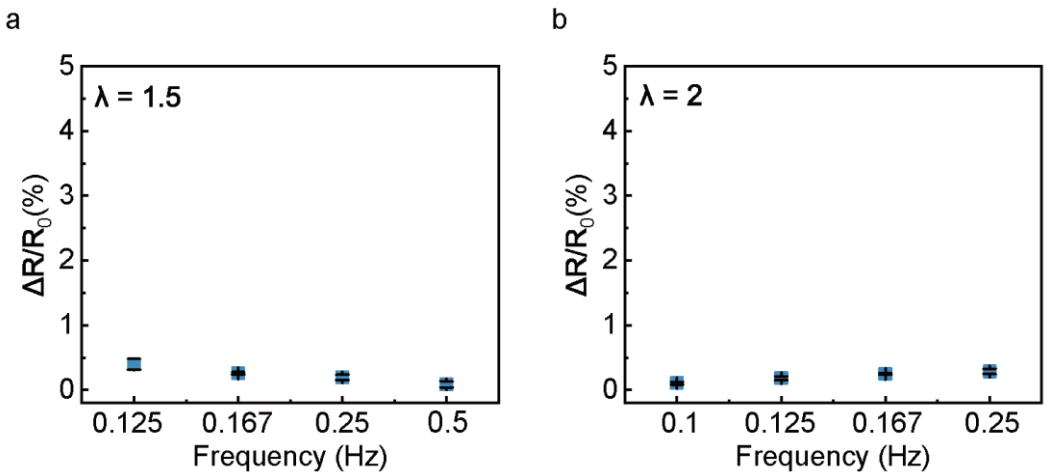


Figure S16. The variation in the gold electrode's electrical conductivity $\Delta R/R_0$ as a function of the frequencies of the applied loading and unloading cycle of the electrical tissue adhesive. (a) λ = 1.5, (b) λ = 2). Values in (a) and (b) represent the mean and the standard deviation (n = 3).

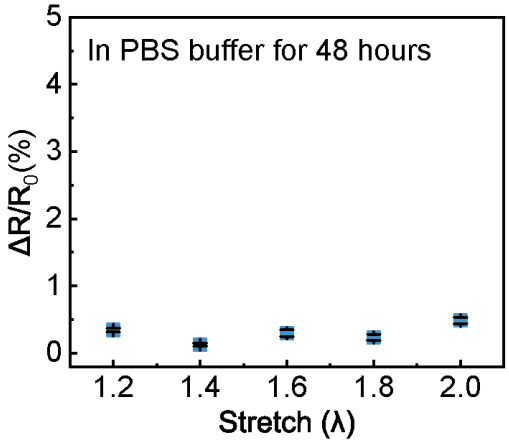


Figure S17. The variation in the gold electrode's electrical conductivity $\Delta R/R_0$ as a function of applied stretch ratios, after the electrical tissue adhesive has been immersed in PBS buffer for 48 hours. Values represent the mean and the standard deviation (n = 3).

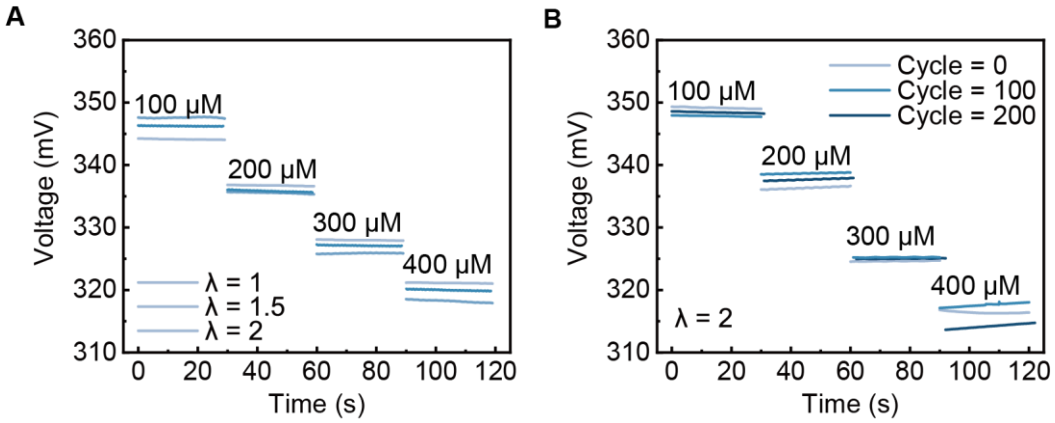


Figure S18. Electrical responses of glucose biosensor subjected to different stretch ratios and cycle nubmers. a) Output voltage as a function of time for the electrical tissue adhesive subjected to different stretch ratios up to 2. b) Output voltage as a function of time for the electrical tissue adhesive subjected to different cycle numbers up to 200.

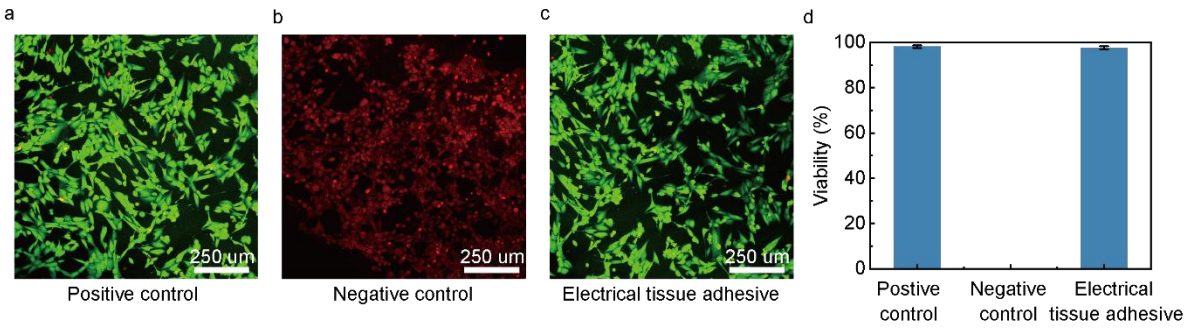


Figure S19. Cell viability was assessed using NIH-3T3 cells. Untreated cells served as the positive control (a), while cells treated with 70% ethanol were used as the negative control (b). Cell viability after 24 h incubation with medium pre-exposed to the electrical tissue adhesive (c). Green fluorescence indicates viable cells, while red indicates dead cells. d) Viability is calculated as the ratio of viable cells to total cells in the images. Values in (d) represent the mean and the standard deviation (n = 4). Scale bars in (a), (b), and (c) are 250 μm.

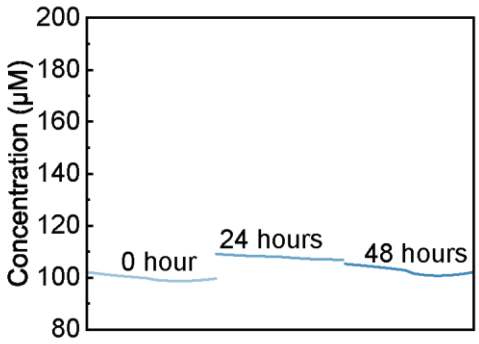


Figure S20. Long-term monitoring of the glucose concentration over 48 hours.

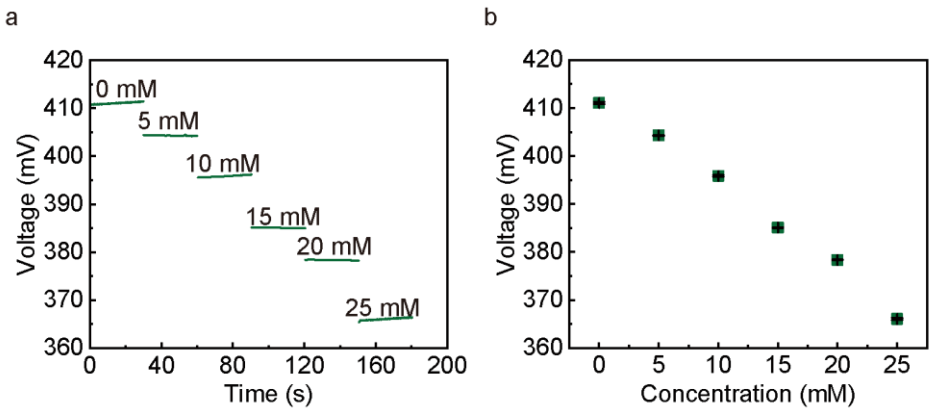


Figure S21. Sensing performance of lactate sensor. a) The output voltage as a function of time corresponding to various lactate concentrations. b) The output voltage as a function of various lactate concentrations. Values in (b) represent the mean and the standard deviation (n = 3).

Table S1. Comparison between the electrical tissue adhesive with conventional tissue-device interfaces.

No.	Adhesive material	Adhesive mechanism	Adhesion strength	Sensing type	Strain sensitivity	Reference
1	Tissue-adhesive Hydrogel	Covalent crosslinking	500 Jm^{-2}	Glucose in sweat	$\Delta R/R_0$ = 1.5 % at stretch =2	This work
2	Bio-adhesive polymer	Covalent crosslinking	30 Jm^{-2}	semiconductors and transistors for electrophysiological recording	0.5 mS at 40 % stretch	[6]
3	Hydrogel	molecular interactions to crosslink polymeric backbones	27 kPa	Tremors and abnormal gait under simulated Parkinson's conditions	10 % change in signal at 90° bending	[7]
4	Conductive hydrogel	Material stickiness	8 kPa	Epidermal electrophysiological signals	$\Delta R/R_0$ = 0.67 at 200 % strain	[8]
5	Conductive hydrogel	Material stickiness	1.5 kPa	Physical signals and joint movements	$(\Delta R/R_0)/\varepsilon$= 0.75 at 200 % strain	[9]
6	Adhesive hydrogel	Catechol groups, electrostatic attraction, and hydrogen bonds	59.7 Nm^{-1}	EEG	NA	[10]
7	Hydrogel	Material stickiness	60 kPa	Physical state of humans during exercise	$\Delta R/R_0$ = 1.03 at 40 % strain	[11]
8	Hydrogel	Material stickiness	24 kPa	Body motion sensing in various scenarios	$\Delta R/R_0$ = 250 % at 90° bending	[12]
9	Hydrogel	Material stickiness	10 kPa	Bending–recovery movement of joints, electrophysiological and body movement signals.	$\Delta R/R_0$ = 50 % at 90° bending	[13]

Note for movie S1

Movie S1: FEA simulating the stress distribution of the electrical tissue adhesive adered with electrode during stretching.

Movie S2: FEA simulating the energy release rate at the interfaces with and without electrical tissue adhesive under stetching.

Reference

[1] T. H. Wong, Y. Liu, J. Li, K. Yao, S. Liu, C. K. Yiu, X. Huang, M. Wu, W. Park, J. J. A. F. M. Zhou, *Advanced Functional Materials* **2022**, 32, 2111269.

[2] H. Yuk, C. E. Varela, C. S. Nabzdyk, X. Mao, R. F. Padera, E. T. Roche, X. Zhao, *Nature* **2019**, 575, 169.

[3] Y. Liu, X. Huang, J. Zhou, C. K. Yiu, Z. Song, W. Huang, S. K. Nejad, H. Li, T. H. Wong, K. Yao, *Advanced Science* **2022**, 9, 2104635.

[4] G. Theocharidis, H. Yuk, H. Roh, L. Wang, I. Mezghani, J. Wu, A. Kafanas, M. Contreras, B. Sumpio, Z. Li, *Nature biomedical engineering* **2022**, 6, 1118.

[5] T. Zhang, S. Lin, H. Yuk, X. Zhao, *Extreme Mechanics Letters* **2015**, 4, 1.

[6] N. Li, Y. Li, Z. Cheng, Y. Liu, Y. Dai, S. Kang, S. Li, N. Shan, S. Wai, A. Ziaja, *Science Advances* **2023**, 381, 686.

[7] A. Roy, S. Zenker, S. Jain, R. Afshari, Y. Oz, Y. Zheng, N. Annabi, *Advanced Materials* **2024**, 2404225.

[8] W. Wang, H. Zhou, Z. Xu, Z. Li, L. Zhang, P. Wan, *Advanced Materials* **2024**, 2401035.

[9] H. Zheng, N. Lin, Y. He, B. Zuo, *ACS Applied Materials & Interfaces* **2021**, 13, 40013.

[10] G. Yang, K. Zhu, W. Guo, D. Wu, X. Quan, X. Huang, S. Liu, Y. Li, H. Fang, Y. Qiu, *Advanced Functional Materials* **2022**, 32, 2200457.

[11] X. Yuan, C. Guo, Z. Wang, H. Jiang, Y. He, J. Xu, B. Guo, *ACS Applied Electronic Materials* **2023**, 5, 1420.

[12] X. Zhang, F. Li, S. Liang, Y. J. C. E. J. Bai, *Chemical Engineering Journal* **2024**, 153385.

[13] J. Sun, X. Wu, J. Xiao, Y. Zhang, J. Ding, J. Jiang, Z. Chen, X. Liu, D. Wei, L. Zhou, *ACS Applied Materials & Interfaces* **2023**, 15, 5897.